12 Neuroradiology: Neoplasms and Epilepsy

Saman Hazany, John Go, Robert W. Henderson, Paul Kim, and Meng Law

Case 12.1: Langerhans Cell Histiocytosis

History

29-year-old female with palpable neck mass.

Findings

Axial post-contrast CT (Fig. 12.1a), FDG-PET (Fig. 12.1b), and PET-CT fusion (Fig. 12.1c) demonstrate hypermetabolic, peripherally enhancing mass inseparable from the posterior parotid gland.

Impression

Biopsy-proven Langerhans cell histiocytosis (LCH).

Pearls and Pitfalls

Differential diagnosis for parotid masses is broad including benign and malignant etiologies. The finding in this case represents involvement of an intra-parotid lymph node. The most common site of involvement by LCH is the bone (90 %) followed by the skin (30 %). FDG-PET is sensitive in detection of multifocal disease and shown to be superior to technetium 99 m methylene diphosphonate bone scans or radiograph in detection of active osseous lesions and response to therapy. There are limited number of studies evaluating utility of FDG-PET in soft tissue involvement by LCH.

P.S. Conti, A. Kaushik (eds.), *PET-CT*, DOI 10.1007/978-1-4419-5811-2_12

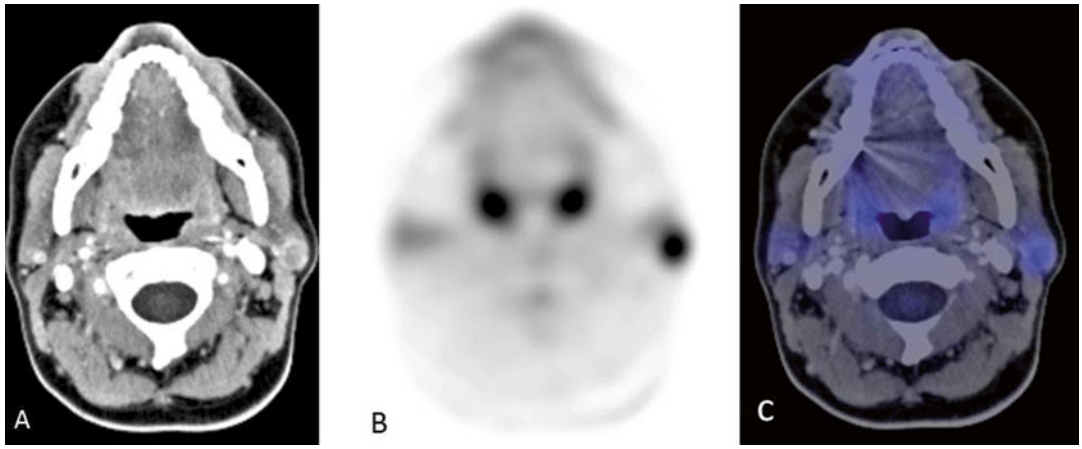

Fig. 12.1

Discussion

LCH is a rare idiopathic "neoplastic" process secondary to monoclonal proliferation of Langerhans-type cells. It is more common in the pediatric population, with a peak incidence between 1 and 3 years of age. There is also a male predilection (M:F 1.2–2.1:1). The course of the disease ranges from spontaneous regression to rapid progression (especially common in young children with multisystem disease). LCH can involve multiple organ systems, single-organ system with multiple sites, or single site. Diagnosis is confirmed histologically by tissue sampling.

The prognosis is variable and depends on disease burden, with single-organ system disease carrying better prognosis than multisystem disease. In 2008 the WHO recommended distinguishing LCH from a more pleomorphic variant know as Langerhans cell sarcoma, which carries a worse prognosis. Treatment ranges from excision or limited radiation for single-focus disease to systemic chemotherapy and steroid administration for multifocal disease and supportive care in cases of endocrine and CNS involvement (Fig. 12.1).

Case 12.2: Crossed Cerebellar Diaschisis

History

43-year-old female with remote history of biopsy-proven oligoastrocytoma within the right cerebral hemisphere status post radiation.

Findings

CT: Areas of calcification with associated volume loss and no appreciable mass effect centered in the right thalamus and internal capsule compatible with known previously treated oligoastrocytoma (Fig. 12.2).

FDG-PET: Relative decreased FDG uptake in the right cerebral hemisphere as compared to left compatible with post radiation change. Relative decreased FDG uptake in the left cerebellar hemisphere as compared to right compatible with crossed cerebellar diaschisis (Fig. 12.2).

MRI: Subtle asymmetric left cerebellar volume loss with no decreased diffusion or signal abnormality (Fig. 12.2).

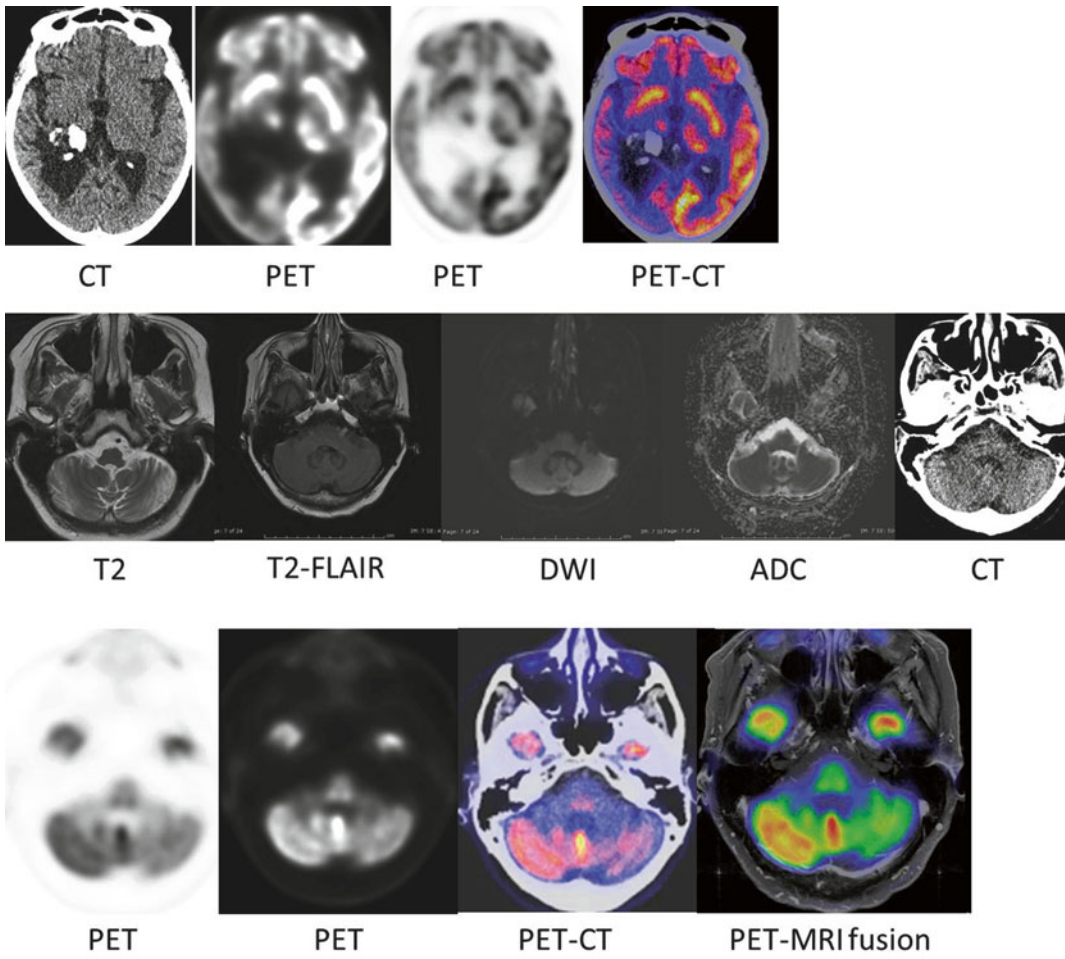

Fig. 12.2

Impression

Crossed cerebellar diaschisis.

Pearls and Pitfalls

Crossed cerebellar diaschisis refers to hypometabolism in a cerebellar hemisphere contralateral to a cerebral hemispheric lesion. Lesions located in the motor cortex, anterior corona radiata, and thalamus (as in this case) produce the most marked suppression of the contralateral cerebellar cortical metabolism. Findings of hypometabolism are seen on FDG-PET. Decreased blood flow to the contralateral cerebellum has also been shown on MR perfusion imaging in setting of MCA territory stroke. In setting of chronic hypometabolism, cerebellar atrophy ensues.

Discussion

Crossed cerebellar diaschisis (CCD) has been reported in patients with ischemic and hemorrhagic hemispheric stroke, during carotid amytal procedure, migraine attack, seizure, space occupying lesion, and focal volume loss of a cerebral hemisphere. CCD is thought to be due to interruption of corticopontocerebellar fibers and subsequent transneuronal metabolic and blood flow alterations that are distant to and on the opposite side of the primary lesion. Border-zone cerebellar infarcts have also been reported in setting of CCD especially in migraines with prolonged aura. In setting of cerebral infarct, CCD is associated with poor clinical outcome (Fig. 12.2).

Case 12.3: Tumor Recurrence/Progression

History

43-year-old female with remote history of treated oligoastrocytoma WHO grade III, within the right cerebral hemisphere status post radiation and chemotherapy about 14 years ago with increased area of enhancement on surveillance MRI (prior MRI is not shown here). Clinical concern for tumor recurrence/progression versus radiation necrosis.

Findings

PET-CT: Focal mass-like area on CT shows abnormal avid FDG uptake which is increased in extent and avidity as compared to prior studies (not shown) (Fig. 12.3).

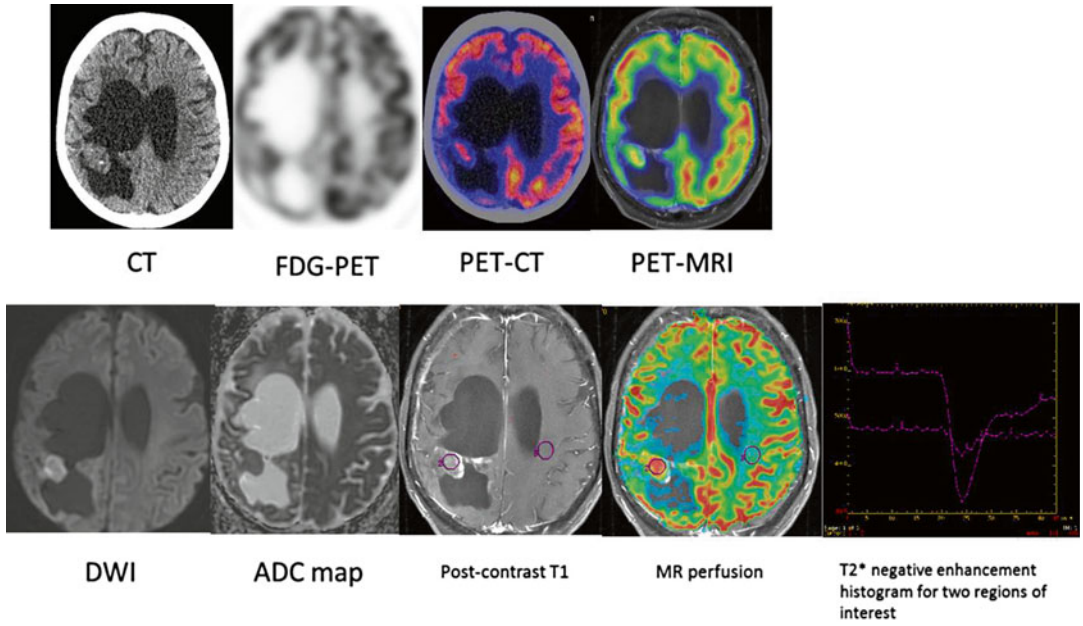

Fig. 12.3

MRI: Approximately 2 cm area of new mild enhancement (prior study not shown) and increased cerebral blood volume (CBV) on dynamic susceptibility contrast-enhanced cerebral blood volume (DSCE-CBV) magnetic resonance imaging (i.e., MR perfusion) with associated decreased diffusion.

PET-MRI: Overlap of abnormality on PET and MRI confirming hypermetabolism and increased CBV (Fig. 12.3).

Impression

Tumor recurrence/progression.

Pearls and Pitfalls

In setting of treated glioma, differentiating radiation necrosis from tumor recurrence/progression on imaging is crucial but often difficult. Findings on conventional imaging are relatively nonspecific and often unable to distinguish the two entities. Utility of fluorodeoxyglucose positron emission tomographic (FDG-PET), which studies tumor metabolism, for differentiation of glioma recurrence/progression from radiation necrosis has been controversial with reported specificities as low as 18 %. However, considering recent advances in MR perfusion imaging, which studies tumor vascularity, combination of the two modalities maybe helpful. These imaging tools have also been for differentiation of high-grade from low-grade tumors and benign lesions.

Discussion

Primary central nervous system neoplasia is one of the most frequent causes of death between 15 and 35 years of age. Gliomas constitute >90 % of primary brain tumors diagnosed after the second decade of life. Despite treatment with chemotherapy and radiation, including proton-beam therapy (PBT) and other radiosurgery, the majority of these tumors progress and/or recur. Moreover, treatment with radiation remains associated with tissue necrosis that may also lead to clinical deterioration. Differentiating recurrent tumor (or progression of tumor) from predominant radiation necrosis has treatment and prognostic implications.

Oligoastrocytomas histologically represent mixed glial cell origin, astrocytoma, and oligodendroglioma with a peak incidence occurring in the third to fifth decade. The incidence among males is higher than females. Prognosis is similar to anaplastic astrocytoma and worsened with increased age of onset, with 5-year survival of greater than 50 % and a 10-year survival of 25–34 %. On histologic evaluation, predominance of oligodendrocytes over astrocytes confers a better prognosis. Treatment is controversial and includes surgical reduction, radiotherapy, and chemotherapy often with corticosteroids and seizure prophylaxis. In our case, surgery was not possible as the tumor was in an eloquent location (Fig. 12.3).

Case 12.4: Stage IVa (T2 N2a M0) Oropharyngeal/ Tonsillar HPV-Positive Squamous Cell Carcinoma

History

42-year-old male with no history of smoking or alcohol consumption presents with neck mass.

Findings

Axial post-contrast CT (A), PET (B), and PET-CT fusion (C) and coronal post-contrast CT demonstrate 2.5 cm FDG-avid mass involving the left palatine tonsil/oropharynx with associated FDG-avid 5.4 cm level 2–4 lymph node (Figs. 12.4 and 12.5). There is also nonspecific FDG uptake in the right palatine tonsil and both sublingual glands, none of which were involved by tumor.

Impression

Stage IVa (T2 N2a M0) oropharyngeal/tonsillar squamous cell carcinoma.

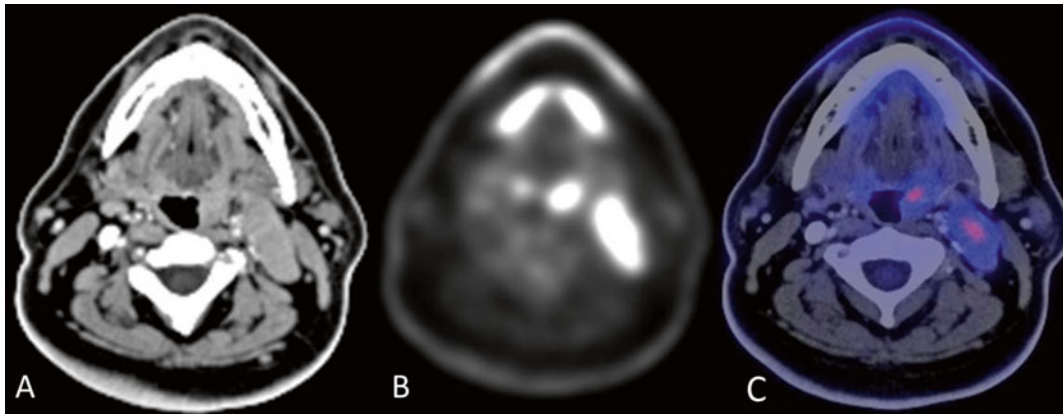

Fig. 12.4

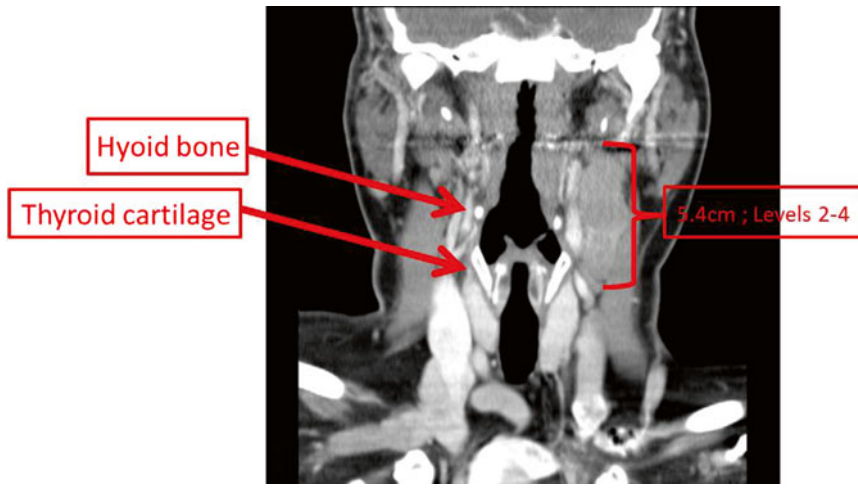

Fig. 12.5

Pearls and Pitfalls

Squamous cell carcinoma (SCC) accounts for the vast majority of malignancies of the oral cavity and oropharynx and is commonly evaluated with radiologic imaging. The symptoms of disease, the routes by which it may spread, and the prognosis vary greatly, depending in large part on the anatomic site at which the primary tumor originates and the stage of the tumor at time of presentation. FDG-PET-CT is used at most centers for detection of otherwise occult primary oropharyngeal SCC (OSCC), as well as determining the local extent and stage of the tumor (including lymph node and distant metastasis). In our case, the tumor was about

2.5 cm with a 5.4 cm ipsilateral lymph node and no distant metastasis, making it T2, N2a, M0, or stage IVA [1]. Tables 12.1 and 12.2 describe TNM staging of oropharyngeal SCC [1].

Discussion

A large body of recent research points out the increasing incidence of human papillomavirus (HPV) as a common cause of oropharyngeal squamous cell carcinoma (OSCC), which includes tonsillar and base of

Table 12.1 TNM staging of oropharyngeal squamous cell carcinoma

Cancer stage	T	N	M
0	Tis	N0	M0
I	T1	N0	M0
II	T2	N0	M0
III	T1, T2, T3	N1	M0
		N0, N1	M0
IVA	T1, T2, T3, T4a	N2	M0
		N0, N1, N2	M0
IVB	Any	N3	M0
	T4b	Any	M0
IVC	Any	Any	M1

Table 12.2 TNM staging of oropharyngeal squamous cell carcinoma

Primary tumor of oropharynx	
Tx	Primary tumor cannot be assessed
T0	No evidence of primary tumor is seen
T1	Primary tumor has a maximal diameter of less than 2 cm
T2	Primary tumor has a maximal diameter of 2–4 cm
T3	Primary tumor has a maximal diameter of more than 4 cm
T4a	Primary tumor involves the larynx, intrinsic or extrinsic muscles of the tongue, medial pterygoid, hard palate, mandible
T4b	Primary tumor involves the lateral pterygoid muscle, pterygoid plates, lateral nasopharynx, skull base, carotid artery
Regional metastasis	
Nx	Regional lymph nodes cannot be assessed
N0	No regional lymph node metastasis is evident
N1	Ipsilateral single enlarged node with a maximal diameter of less than 3 cm
N2a	Ipsilateral single enlarged node with a maximal diameter of 3–6 cm
N2b	Ipsilateral multiple enlarged nodes with a maximal diameter of less than 6 cm
N2c	Bilateral or contralateral enlarged nodes with a maximal diameter of less than 6 cm
N3	Enlarged node with a maximal diameter if more than 6 cm
Distant metastasis	
M0	No distant metastasis is evident
M1	Distant metastasis is evident

tongue cancer. Approximately 25 % of all head and neck cancers and 60 % of all oropharyngeal cancers are HPV positive. This data has made HPV an independent risk factor for OSCC, in addition to smoking and alcohol consumption. Patients with HPV-positive cancer have their first sexual experience at a young age and have multiple partners, suggesting that increased incidence of OSCC in the United States and some countries in northern Europe is because of a new, primarily sexually transmitted HPV epidemic. Oral and vaginal sex and open-mouth kissing have been associated with increased incidence of HPV-associated OSCC. There are >100 HPV types, some found in skin warts and others in mucous tissues. HPV-16 accounts for 90–95 % of HPV-positive OSCC. HPV-associated OSCC has a better prognosis than other types of OSCC, and the knowledge of this association can alter treatment planning. There are no accurate radiologic features to confidently distinguish this entity, but cystic adenopathy (not seen in our case) has been associated with HPV-positive OSCC (Figs. 12.4 and 12.5).

Case 12.5: Adenoid Cystic Carcinoma Recurrence

History

42-year-old female with history of adenoid cystic carcinoma involving the right maxillary sinus status post resection and XRT 13 years ago.

Findings

Axial post-contrast fat-saturated T1 (Fig. 12.6a), T2 (Fig. 12.6b), PET (Fig. 12.6c), PET-MRI fusion (Fig. 12.6d) and coronal non-contrast CT (Fig. 12.6e), and PET-CT fusion (Fig. 12.6f) of the face show enhancing, FDG-avid mass within the right masticator space.

Impression

Adenoid cystic carcinoma recurrence.

Pearls and Pitfalls

The clinical utility of ^{18}F-FDG-PET in evaluating salivary gland malignancies has not been well defined. In a study of 34 patients with newly diagnosed salivary gland cancers, ^{18}F-FDG-PET was more sensitive than CT for the detection of primary salivary gland tumors and cervical metastases [2]. High-grade malignancies had higher mean maximum SUVs than did low- and intermediate-grade malignancies. In a 25 months follow-up,

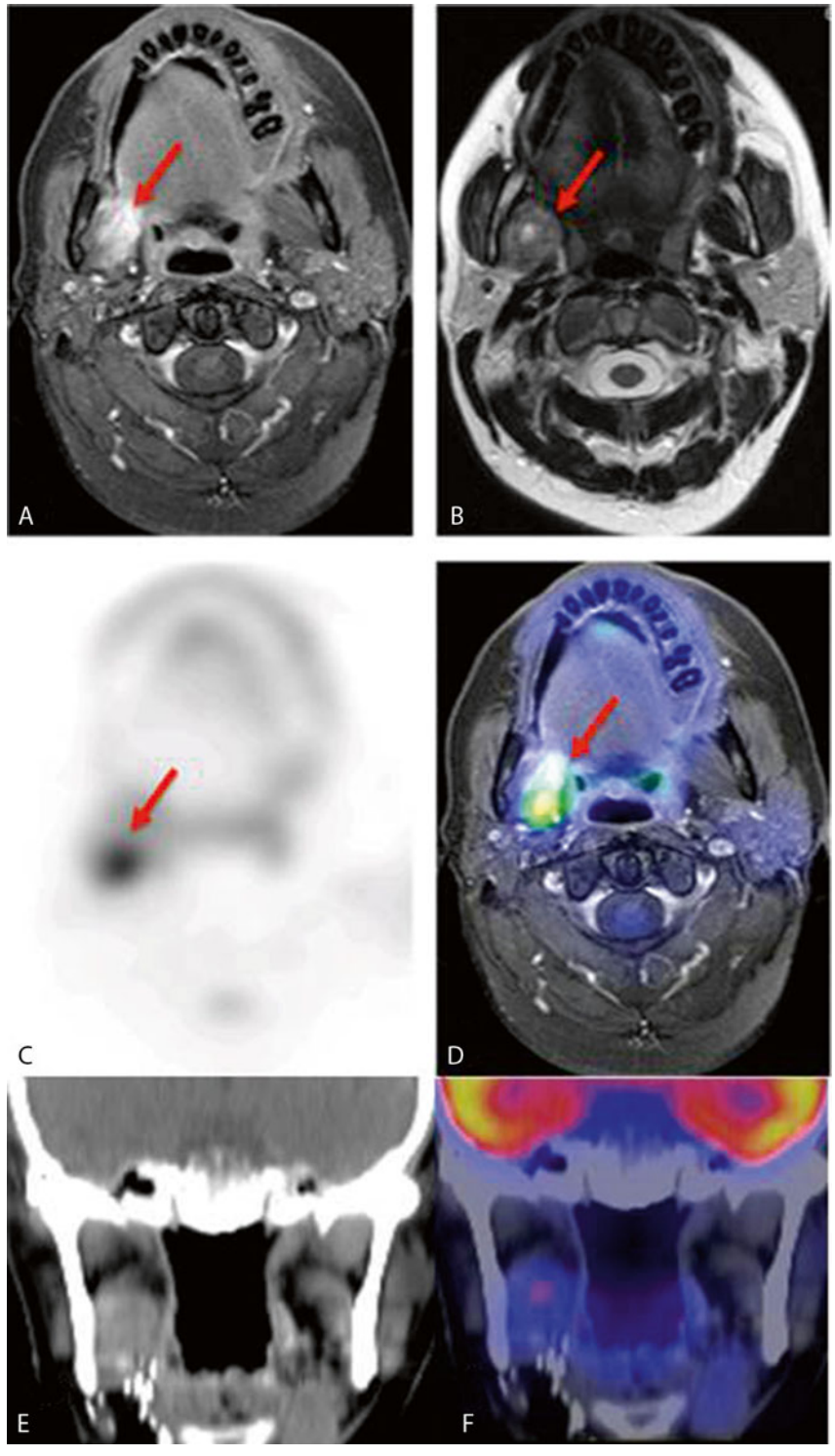

Fig. 12.6

^{18}F-FDG-PEt also correctly diagnosed local-regional recurrences in six patients and new distant metastases in nine patients.

Occasional failure of ^{18}F-FDG-PET in detecting some primary salivary gland tumors has been attributed to normal physiologic uptake of ^{18}F-FDG in the head and neck region, including the salivary glands, and small size of some of the tumors.

Discussion

Adenoid cystic carcinoma most often occurs in the salivary glands, but has also been reported in the breast, lacrimal glands, lung, brain, Bartholin glands, trachea, and paranasal sinuses. It is the third most common malignant salivary gland tumor overall (after mucoepidermoid carcinoma and polymorphous low-grade adenocarcinoma). It represents 28 % of malignant submandibular gland tumors, making it the single most common malignant salivary gland tumor in this region. Salivary gland malignancy is currently managed primarily by resection of the primary tumor, possibly in combination with neck dissection or subsequent radiotherapy. Proper management requires accurate information about the site and extent of tumors (Fig. 12.6).

Case 12.6: Right Vocal Cord Paralysis

History

34-year-old female with recurrent papillary thyroid carcinoma, status post thyroidectomy, and neck dissection with hoarseness.

Findings

Axial FDG-PET (Fig. 12.7a), non-contrast CT (Fig. 12.7b), PET-CT fusion (Fig. 12.7c), axial T1-weighted MRI (Fig. 12.7d), and PET-MRI fusion (Fig. 12.7e) images of the neck demonstrate asymmetric uptake in the left cricoarytenoid muscle.

Axial CT at the level of the vocal cords (Fig. 12.7f) shows subtle medialization of the right vocal fold.

Impression

Right vocal cord paralysis.

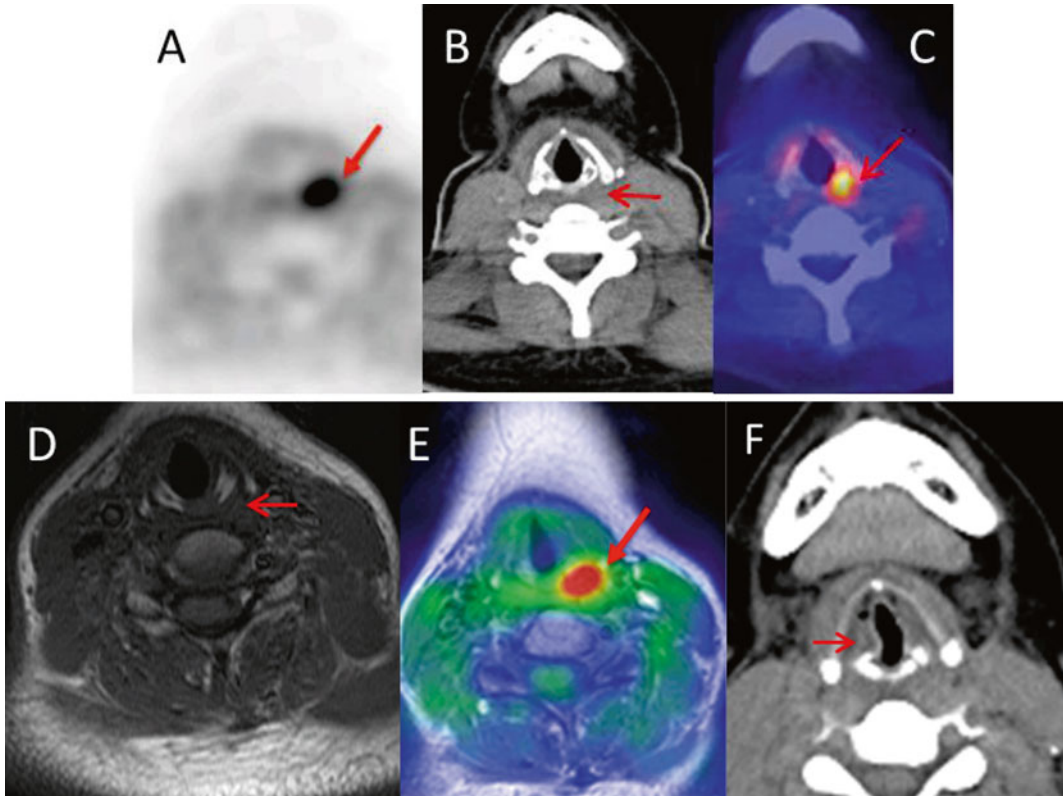

Fig. 12.7

Pearls and Pitfalls

Incidence of permanent recurrent laryngeal nerve (RLN) injury after thyroid surgery is 1–2 % when performed by experienced neck surgeons and higher in hands of less experienced surgeon or in setting of malignant disease. In some cases of thyroid malignancy, the nerve is purposely sacrificed when it runs through the tumor.

Up to 40 % of individuals with vocal cord paralysis may be asymptomatic, making detection of this entity on imaging essential, as vocal cord paralysis can be an initial sign of invasion or compression of the RLN. Detection of vocal cord paralysis can be difficult on conventional imaging (MRI or CT), however usually easily seen on PET. Knowledge of laryngeal anatomy helps the radiologist differentiate this entity from metastatic disease and/or lymphadenopathy.

Discussion

Understanding the anatomy of RLN helps the radiologist in determining the cause of vocal cord paralysis. The vagus nerve descends along the course of the carotid artery into the upper mediastinum bilaterally. The right RLN exits from the vagus nerve anterior to the subclavian artery and

courses posteriorly under the artery at the level of the brachiocephalic bifurcation and courses obliquely toward the right tracheoesophageal groove. The left RLN exits from the vagus nerve at the level of the aortic arch, then courses posteromedially beneath it, and thus passes through the aorticopulmonary window posterior to the ligamentum arteriosum. It then ascends vertically through the superior mediastinum to reach the tracheoesophageal groove. Both RLNs enter the larynx posterior to the cricoarytenoid joints and innervate the intrinsic laryngeal muscles [3] (Fig. 12.7a–f).

Case 12.7: Focal Cortical Dysplasia (ILAE Type IIa)

History

12-year-old male with epilepsy.

Findings

Dysplastic thickened cortex in the superior-medial left parietal lobe with associated subtle signal abnormality on FLAIR and decrease metabolic activity on PET in the interictal state (Figs. 12.8 and 12.9).

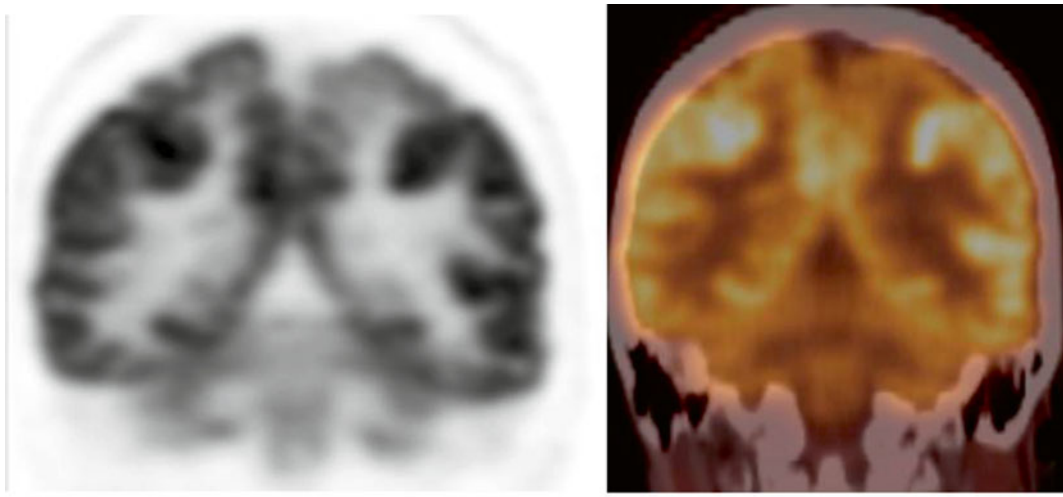

Fig. 12.8

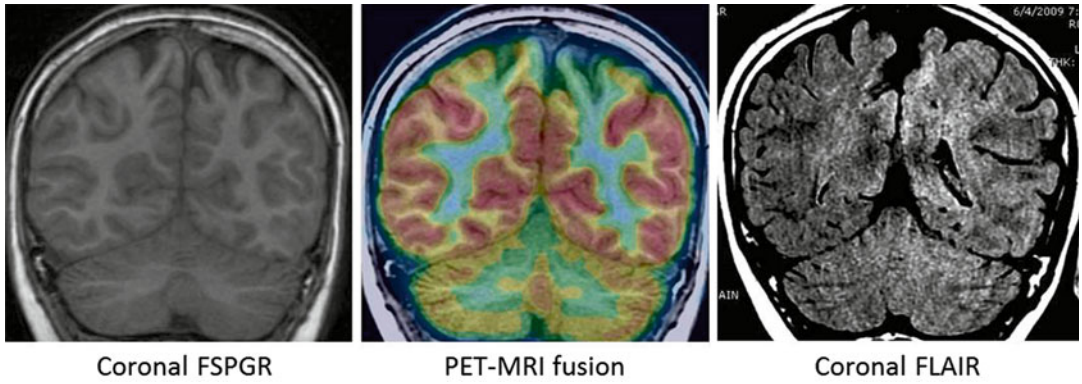

Fig. 12.9

Impression

Focal cortical dysplasia (ILAE type IIa).

Pearls and Pitfalls

FDG-PET/MRI coregistration has been shown to be useful in detecting cortical dysplasia in patients with epilepsy [4]. The addition of FDG-PET/MRI coregistration to the presurgical protocol enhances the ability to detect FCD, especially in patients with type I or type II FCD and non-concordant EEG and MRI findings. Sensitivity of MRI for the detection of FCD has been reported in 53–90 % of patients with surgically proven FCD. An increase in the detection of hypometabolism at the location of the lesion on FDG-PET images when using FDG-PET/MRI coregistration has been shown and considered a useful technique in the presurgical protocol to improve detection of the epileptogenic lesion.

Focal cortical dysplasia is a disorder of cortical formation, which may demonstrate both architectural and proliferative features, and a frequent cause of epilepsy. MR findings of FCD are related to the histologic grade of FCD. Most common finding of FCD on MRI, which is usually seen in severe cortical dysplasia, is indistinct gray-white matter demarcation with T2 prolongation involving the subcortical white matter. FDG-PET is more sensitive in the detection of grades I and II FCD. The histologic abnormalities of bizarre glial cells (balloon cells), ectopic neurons, and abnormalities of myelination may be responsible for the MR abnormality in blurring of the gray-white matter junction with abnormal signal intensity of the subcortical white matter. FCD has been histologically divided into three histologic types by International League Against Epilepsy (ILAE). ILAE type IIa is histologically characterized by cortical dyslamination and dysmorphic neurons without balloon cells (Figs. 12.8 and 12.9).

Case 12.8: Left Medial Temporal Sclerosis

History

22-year-old female with epilepsy scanned in interictal state.

Findings

Coronal PET (Fig. 12.10a), PET-CT fusion (Fig. 12.10b), and PET-MRI fusion (Fig. 12.10c) images show asymmetric decrease in FDG uptake in the left medial temporal lobe (including parahippocampal gyrus) and hippocampus.

Coronal FLAIR image at the level of hippocampal body-tail (Fig. 12.10d) shows small left hippocampus with abnormal configuration and hyperintense signal on FLAIR, characteristic of medial temporal sclerosis.

Impression

Left medial temporal sclerosis.

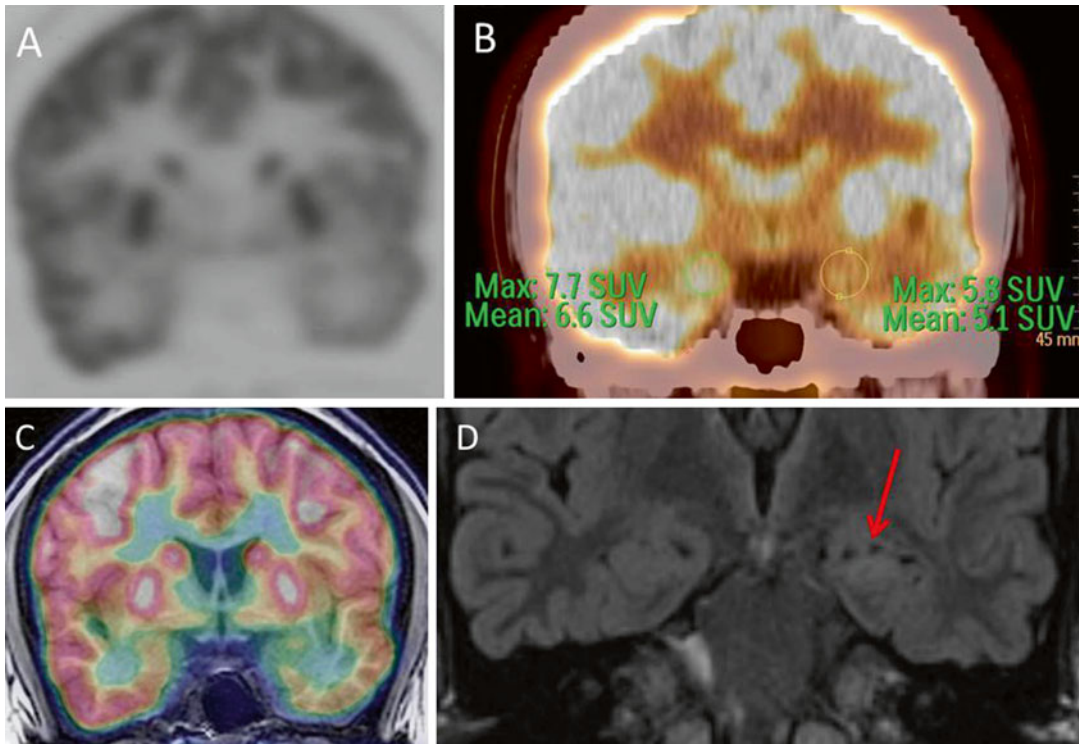

Fig. 12.10

Pearls and Pitfalls

The ultimate goal of PET in epilepsy imaging is to identify and/or confirm the location of a seizure focus which may be completely or partially invisible to other diagnostic techniques (EEG, MRI). PET is generally performed in the interictal state and demonstrates decrease metabolic activity in the epileptogenic focus. Anterior temporal lobe resection has been reported to increase quality-adjusted life expectancy by 7.5 quality-adjusted life years and is the preferred treatment in setting of medial temporal lobe epilepsy. PET imaging and PET-MRI fusion combined with assessment of seizure semiology and extracranial and intracranial EEG findings help the neurosurgeon in determining the extent of epileptogenic focus.

Discussion

Mesial temporal sclerosis (MTS), most common pathological abnormality in temporal lobe epilepsy, is a specific pattern of hippocampal neuron cell loss with associated hippocampal atrophy and gliosis. Cell loss can occur in CA1 and CA4, CA4 alone, or CA1 to CA4 segments. It can be a primary epileptogenic focus or secondary to other epileptogenic focus in the same cerebral hemisphere. PET is useful in determining the location and extent of epileptogenic focus. MRI findings of MTS include small-size, abnormal configuration (including loss of hippocampal head interdigitations) and T2 prolongation or increased FLAIR signal in the hippocampus (Fig. 12.10a–d).

Case 12.9: Sydenham's Chorea

History

11-year-old female with mood change, hearing voices, dysarthria, and choreoathetosis of four extremities. No significant past medical history or family history and no recent infections, pharyngitis, or strep throat. Her brain MRI was unremarkable.

Findings

Axial FDG-PET (Fig. 12.11a), CT (Fig. 12.11b), and PET-CT fusion images (Fig. 12.11c) at the level of the basal ganglia demonstrate symmetric marked increased FDG uptake in caudate and putamen, compatible with Sydenham's chorea. Normal metabolic activity is seen in the remaining brain. Figure 12.11d is an example of normal FDG uptake at the level of basal ganglia.

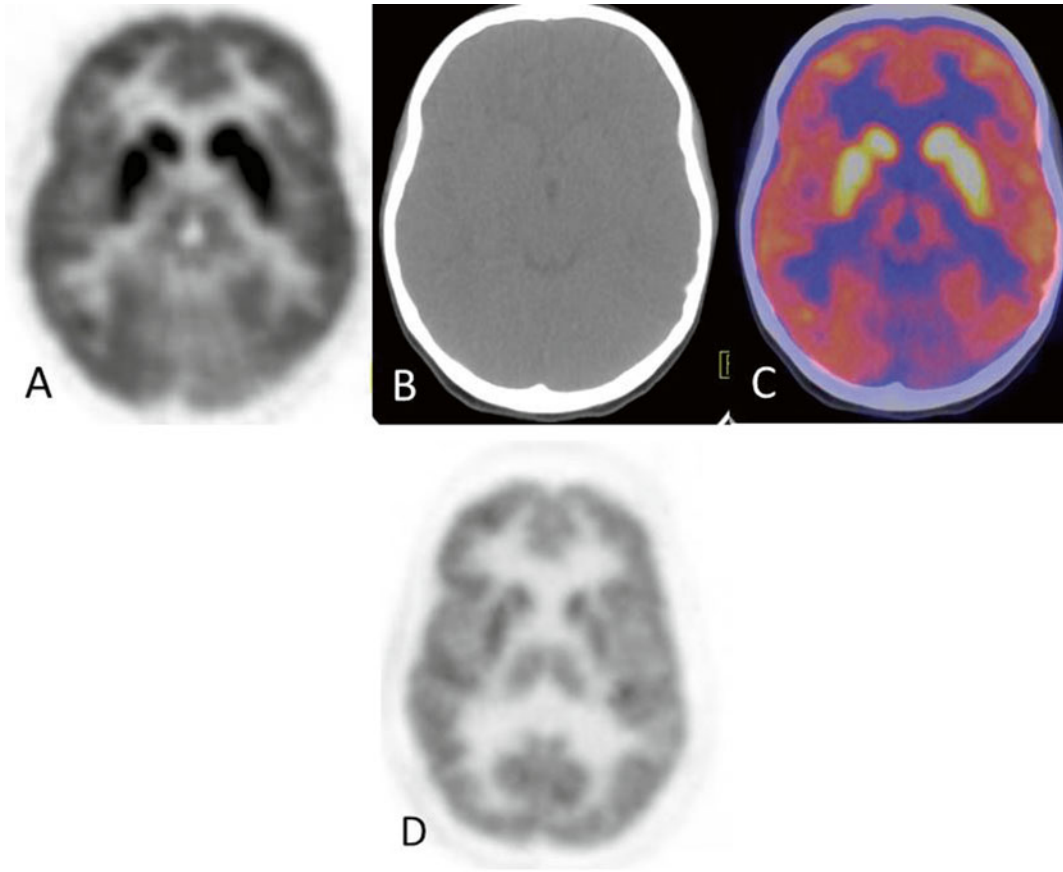

Fig. 12.11

Impression

Sydenham's chorea.

Pearls and Pitfalls

Sydenham's chorea is a late manifestation of rheumatic fever and associated with group A-hemolytic streptococcus. Sydenham's chorea is most common in children and adolescents above the age of 5 (80 %) and twice as common in girls as compared to boys. Preceding or concurrent throat cultures for hemolytic streptococcus can be negative. It is associated with subsequent cardiac valvular heart disease and obsessive-compulsive disorder. A link between multiple tics, pediatric autoimmune neuropsychiatric disorders associated with streptococcal infection (PANDAS syndrome), Tourette syndrome, and Sydenham's chorea has also been suggested.

FDG-PET demonstrates hypermetabolism of the basal ganglia in active Sydenham's chorea. Single-photon emission computed tomography

demonstrates hyperperfusion of the basal ganglia. Magnetic resonance imaging (MRI) studies of patients with active Sydenham's chorea have shown no specific abnormality, but increased size of the caudate, putamen, and globus pallidus has been noted.

Discussion

Recent studies have suggested immunoreactivity as an explanation for Sydenham's chorea. Serum antibodies appear to be an M1 isozyme of pyruvate kinase, which is enriched in the striatum. An initial antibody response to the M streptococcal protein likely cross-reacts with basal ganglia pyruvate kinase. This theory explains the utility of plasmapheresis for treatment in severe Sydenham's chorea. The loss of the hypermetabolic basal ganglia findings in recovery can help explain lack of long-term permanent neurologic sequelae [5] (Fig. 12.11a–d).

References

1. Trotta BM, Pease CS, Rasamny JJ, Raghavan P, Mukerjee S. Oral cavity and oropharyngeal squamous cell cancer: key imaging findings for staging and treatment planning. Radiographics. 2011;31(2):339–54.
2. Roh JL, Ryu CH, Choi SH, Kim JS, Lee JH, Cho KJ, Nam SY, Kim SY. Clinical utility of 18F-FDG for patients with salivary gland malignancies. J Nucl Med. 2007;48(2):240–6.
3. Aquino SL, Duncan GR, Hayman LA. Nerves of the thorax: atlas of normal and pathologic findings. RadioGraphics. 2001;21:1275–81.
4. Goffin K, Van Paesschen W, Dupont P, Baete K, Palmini A, Nuyts J, Van Laere K. Anatomy-based reconstruction of FDG-PET images with implicit partial volume correction improves detection of hypometabolic regions in patients with epilepsy due to focal cortical dysplasia diagnosed on MRI. Eur J Nucl Med Mol Imaging. 2010;37(6):1148–55. Epub 2010 Mar 20.
5. Ho L. Hypermetabolism in bilateral basal ganglia in Sydenham chorea on F-18 FDG PET-CT. Clin Nucl Med. 2009;34(2):114–6.